Ammonia gas sensing characteristics of V_2O_5 nanostructures: A combined experimental and *ab initio* density functional theory approach

A.A. Akande[a,b,*] T. Mosuang[a], C.N.M. Ouma[c], E.M. Benecha[d], T. Tesfamicheal[e], K. Roro[f], A.G.J. Machatine[g], B.W. Mwakikunga[h,i]

[a]University of Limpopo, Department of Physics, P/Bag X1106, Sovenga, 0727, South Africa

[b]CSIR NextGen Enterprises and Institutions, Advanced Internet of Things, P O Box 395, Pretoria, 0001, South Africa

[c]HySA-Infrastructure, North-West University, Faculty of Engineering, Private Bag X6001, Potchefstroom, 252, South Africa

[d]School of Interdisciplinary and Graduate Studies, University of South Africa, UNISA, 0003, Pretoria, South Africa

[e]Science and Engineering Faculty, Queensland University of Technology, 2 George Street, Brisbane, 4000, QLD, Australia

[f]R&D Core-Energy, Council for Scientific and Industrial Research, P O Box 395, Pretoria, 0001, South Africa

[g]Department of Physics, University of Pretoria, Pretoria, 0002, South Africa

[h]DST/CSIR National Centre for Nano-Structured Materials, P O Box 395, Pretoria, 0001, South Africa

[i]Department of Physics, Tshwane University of Technology, P.O. Box 680, Pretoria, 0001, South Africa

*Corresponding author. University of Limpopo, Department of Physics, P/Bag X1106, Sovenga, 0727, South Africa. amos.akande@ul.ac.za

Abstract

A combined experimental and density functional theory of α-V_2O_5 for ammonia gas sensing have been investigated. The material was synthesized from hydrated NH_4VO_3 in CVD at 400 °C in N_2 atmosphere for different time (12 h and 24 h). Highly crystalline orthorhombic α-V_2O_5 nano-rods with dominant (001) and (110) planes/facets nano-rods were observed from XRD, SEM and TEM characterizations. Using VSM technique, para-to ferro-magnetic transition was observed in the α-V_2O_5 nanoparticles synthesized at 24 h. Improved gas sensing was observed in case of the paramagnetic α-V_2O_5 nano-rods (nanoparticles synthesized at 12 h) compared with the one synthesized at 24 h. Additionally, significant rise in gas sensing response was observed around the metal to insulator transition temperature. Calculation of adsorption of NH_3 molecule(s) on (001), (110), (200) and (400) facets showed that (001), (200) and (400) possessed more active sites than (110) surface. However, at higher concentration of NH_3 molecules, the number of adsorbed molecules was found to be limited by the available adsorption sites in the case of (001) thereby causing the surface to be unstable. DFT calculations were also used to investigate NH_3 adsorption on (110) surface of α-V_2O_5 with the analysis showing exponential decrease in the electronic band gap of the material's surface with the increasing numbers of NH_3 loadings.

Keywords: α-V_2O_5; Para-to ferro-magnetic transition; NH_3 adsorption; NH_3 sensing; Electronic band gap

1 Introduction

Vanadium pentoxide (V_2O_5) bulk and nanostructures have been extensively investigated for their catalysis, lithium ion battery, electrochromic and gas sensing applications over the years [1–6]. Their extensive applications can be attributed to the layered structural property of V_2O_5 which makes it easy to embed both organic and inorganic molecules [7,8]. Orthorhombic V_2O_5 belongs to space group, P*mmn* (D_{2h}^{13} No. 59) with lattice parameters a = 3.563 Å, b = 4.369 Å and c = 11.510 Å. Under ambient conditions, orthorhombic V_2O_5 is usually thermodynamic favoured when b and c lattice parameters are flipped hence its use for room temperature application [9–14].

Orthorhombic V_2O_5, like other vanadium oxide polymorphs, exhibits a Mott Hubbard's metal-to-insulator transition (MIT) at temperature of ~375 °C [4] with no structural change making it attractive for many applications. Orthorhombic V_2O_5 contains two atoms of vanadium V located at same 4*f* Wyckoff position with cite symmetry C*s* [14,15], and three atoms of oxygen at different Wyckoff positions and site symmetries (two at 4*f* Wyckoff position with site symmetry C*s* and one at 2a Wyckoff position with cite symmetry of C_2v [14]). Additionally, the coordination of atoms in V_2O_5 has been proven as useful in evolving catalytic reactions and rechargeable batteries among other novel applications [14–18].

As chemical probe, V_2O_5 materials have been used for gas sensing applications due to their capability to adsorb/desorb molecules including ammonia, hydrogen, nitrogen oxides, carbon oxides, hydrocarbon and many volatile organic molecules [4–6,19–21]. These studies have also observed that it is the V_2O_5 atomic structure, valence state and oxygen coordination and vacancy that accounts for its gas sensing ability. However, similar to its metal oxide counterparts, the need for improved sensitivity and selectivity has

hampered the design and manufacture of practical sensing devices. The aim of this current work is to investigate theoretically and experimentally the surface properties of V_2O_5 for ammonia gas sensing. Theoretical calculations of adsorption energies, charge density differences and electronic band structure analysis of different ammonia-adsorbed cleaved surfaces have been considered as selectivity indicators. The typical coordination of Orthorhombic V_2O_5 structure, represented in Fig. (1a), and the *ab initio* simulated structure in Fig. (1b) (courtesy of materials project and BIOVIA materials studio) showed the chain and layer characteristics of the material. Each oxygen atoms possessed different coordination with the centred atom; vanadium, having different bond lengths and Brönsted sites resulting to three structurally different lattice oxygen [22].

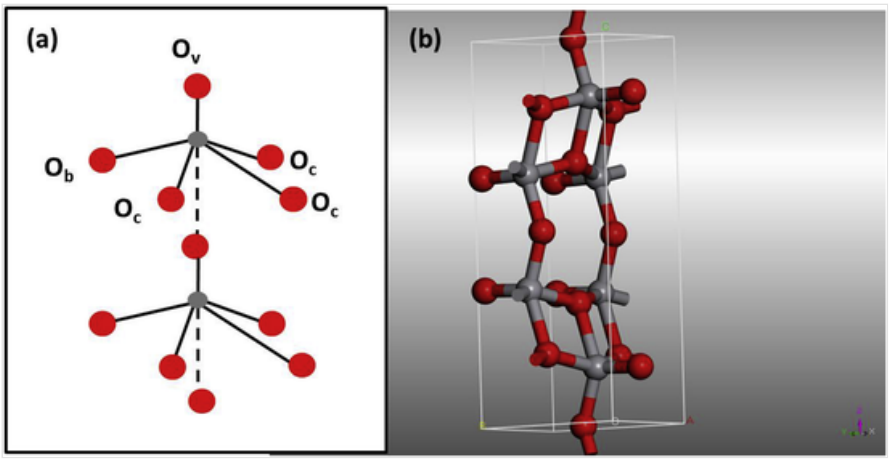

Fig. 1. a) Local coordination of vanadium and oxygen atoms. The grey and red ball(s) are the V and O atoms respectively. O_v – vanadyl oxygen, O_b – bridge oxygen and O_c – chain oxygen respectively. (b) Orthorhombic crystal structure.

2 Materials and methods

2.1 Synthesis and characterization of V_2O_5 nanorods

Following the decomposition of precursor NH_4VO_3 and phase evolution studies of vanadium oxides reported in our previous manuscript [4], thermodynamic and structural parameters of V_2O_5 nanostructure was selected for this study. Here, an amount of NH_4VO_3 was heat-treated during solid-state reaction in a furnace at 400 °C for 12 h and 24 h sampling time in nitrogen atmospheric conditions. The resulting nano-powders were characterized to extract their crystal structural information using Panalytical XPERT PRO PW3050/50 diffractometer with CuKα radiation (45 kV, 400 mA, $\lambda = 0.1540598$ nm and $5° \leq 2\theta \leq 90°$). Microstructure studies were carried out using JEOL 2100 Transmission Electron Microscopy (TEM) (from Tokyo Japan) equipped with a LaB6 filament and a Gartan U1000 camera of 2028 × 2028 pixels, and a high quality in-built Energy dispersive X-ray spectroscopy (EDS) set-up. Magnetic characterization was performed using

Lakeshore 735 vibrating sample magnetometer (VSM) at room temperature. BET analysis of the samples was performed using Trister II micromeritics.

2.2 Gas sensor fabrication and testing

The gas sensor fabrication and testing were carried out using KSGA565 KENOSISTEC instrument from Italy. The sensing electrodes were prepared by ultrasonically dispersing the nanoparticles in the organic solvent for 30 min and later drop casting the solution onto an Al_2O_3–Pt interdigitated electrode (IDE) with heating terminal at the reverse side. The sensor's electrodes were dried at ~ 70 °C in an electric oven for 1 h to ensure thin film deposition of the nanoparticles. Finally, the sensing data were acquired by monitoring changes in electrical currents (i.e electrical current of the sensor material when in the presence of the analyte gas minus the one in the absence of such a gas) for various concentrations of the target analyte or gas molecules using the Keithley pico-meter source meter. Fig. 2 present the schematic arrangement of the sensing peripherals.

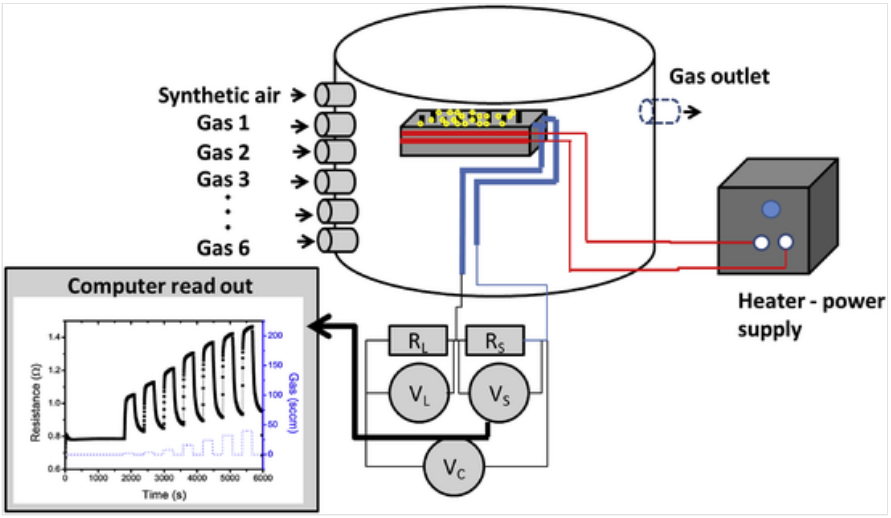

Fig. 2. Schematic diagram of KSGA565 KENOSISTEC sensing station illustrating how the gas sensing measurement was performed.

The sensor's response is determined by measuring the voltage changes of the load resistance. According to the figure, the electronic circuit displays of the gas sensor's element showed R_L, which is the load resistor connected in series with the sensor's element ($R_L = (V\text{-}V_S)/I$) and with a value of 5MΩ. V, is the voltage on the R_L, $V_S = V_C - IR_L$, represent the sensor's signal voltage. V_C is a constant voltage applied on the R_L and sensor's element (having a value of 3 V in this experiment) and finally, R_S is the sensor's resistance ($R_S = V_S/I$).

2.3 Computational details

First principles thermodynamic *ab initio* calculations were performed within the formalism of density functional theory (DFT), as implemented in the CASTEP [23]. All calculations adopted the Perdew-Burke-

Ernzerhof generalized gradient approximation [24] the (GGA-PBE) functional for treating the exchange-correlation effects, while valence-core interactions were approximated by the Vanderbilt ultrasoft pseudopotentials [25]. Full relaxation and geometry optimization and electronic structure calculations were carried out using a bulk orthorhombic V_2O_5 unit cell (space group P*mmn* (D_{2h}^{13} No. 59)) with lattice parameters a = 3.563 Å, b = 4.369 Å and c = 11.510 Å. Adsorption calculations were performed using adsorption locator [25,26] by cleaving (001), (110), (200) and (400) surfaces (all chosen based on experimental XRD characterization results in Fig. 3) of the optimized V_2O_5 primitive unit cell. For each of the cleaved surfaces, a 2 × 2 supercell was constructed to allow large adsorption surface area. A uniform vacuum spacing of 20 Å was allowed in the z-direction to minimize surface-image interaction, after which fully relaxed NH_3 molecules were allowed to interact with each of the surfaces.

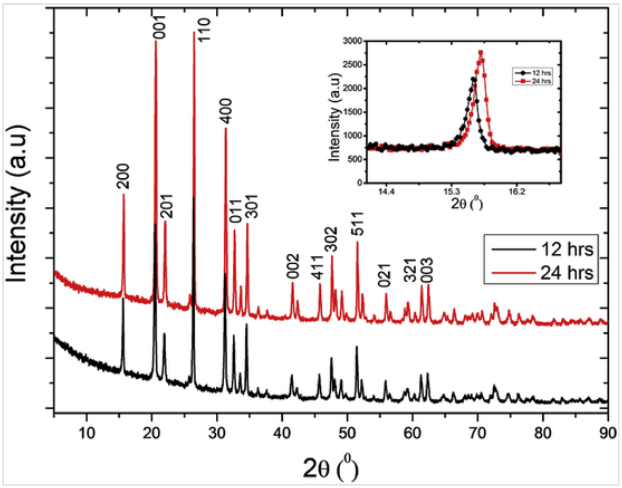

Fig. 3. (a) XRD spectral of the nanopowders samples prepared at 12 and 24 h. Insert is the magnified spectral of the diffraction plane (200).

3 Results and discussion

X-ray diffraction spectra of the sample annealed at 400 °C for 12 h and 24 h are shown in Fig. 3. According to the ICDD (the institute of crystallographic and diffraction database) with powder diffraction number of PDF #41–1426, both samples showed highly crystalline orthorhombic phase of V_2O_5 particles. The spectral showed Braggs positions with strong correlation with the V_2O_5 structure when matched in the Jade 6 software. Among the diffraction planes present in the samples, (001) and (110) were found to be dominant with strong intensities indicating that the majority of the nanoparticles are oriented in (001) and (110) planes or facets. Average crystallite size and micro/nano strain analyses of the nanoparticles were achieved using Debye Scherrer's and Williamson-Hall's relations and shown in Table 1. This analyses showed that the sample annealed at 24 h has larger crystallites with bigger strain compared with the one annealed for 12 h This calculation is clearly supported by the XRD patterns and the inserted magnified peak of the (200) plane in Fig.

3 which showed that the sample annealed for 24 h shifted to the higher angle by about 0.15°. Physical consequences where such observation could be originated from are changes in lattices parameters (distortion in the crystal structure) and strain gradient, which is caused by the stress on the nanoparticles. This showed that the effect of the long period of annealing has slightly deformed the nanoparticles prepared for 24 h. The morphology characterization by SEM and TEM in Fig. 4 showed nano-rod particles formation from bundles of sheets and platelets of V_2O_5 structure. The sample prepared for 24 h showed more crystallinity in its high resolution TEM image (Fig. 4 (d)) and the elemental technique, EDX spectrum which clearly revealed the constituents and qualities of the chemicals involved in the materials is presented in Fig. 4 (e).

Table 1. Summary of crystallite size, strain, magnetic properties and BET surface area of the nanopowders samples prepared at 12 h and 24 h.

Samples	**Particle Size (nm)**	**Strain**	**SaturationMagnetization (*Ms*) (emu/g)**	**Remanence Magnetization (*Mr*) (emu/g)**	**Coercivity, (Hci) (Oe)**	**BET surface area (m^2/g)**
12 h	66	3.55E-04	0.427	0.029	84.658	7.838
24 h	72	3.79E-04	0.724	0.213	292.42	9.607

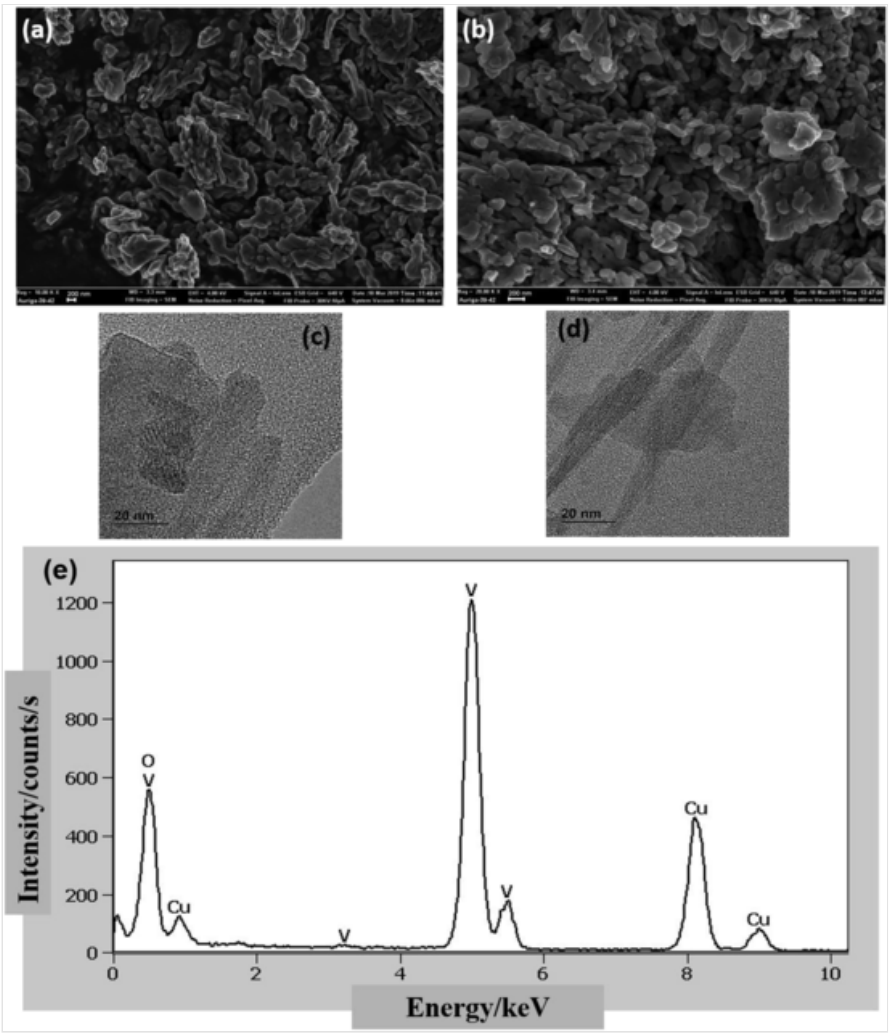

Fig. 4. SEM and TEM profiles of the nanopowders prepared at 12 and 24 h respectively, (a) and (b); SEM, (c) and (d); TEM, (e) is the representative EDX spectrum of the samples.

The M-H hysteresis curve of the samples and the summaries of the magnetic analysis presented in Fig. 5 and Table 1 showed an improved magnetic properties like remanence magnetization, saturation magnetization and magnetic coercivity for the sample annealed for 24 h. Even though, both samples generally demostrated superparamagnetic characteristics in the M-H curve by showing narrow hysteresis widths and saturation at the tips of the curve contrary to the usual paramagnetic behaviour of vanadium oxide, the sample annealed for 24 h displayed superior magnetic properties. This further show a transition in the case of the sample annealed for 24 h from parallel non-interacting and randomly oriented spins (paramagnetic state) to slightly alignment of moments (say ferromagnetic state).

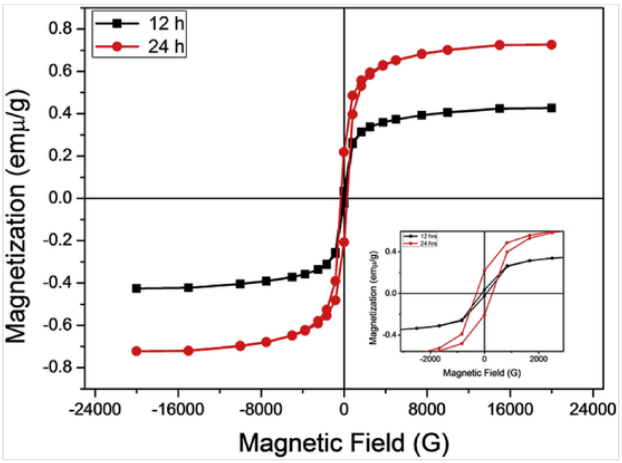

Fig. 5. VSM profiles of the nanopowders samples prepared at 12 and 24. Insert is the magnified image of Fig. 2.

The experimental adsorption and desorption properties according to the BET procedure is presented in Fig. 6 with surface area of 7.838 and 9.607 m^2/g for samples prepared at 12 and 24 h respectively. These BET surface areas fit were performed in partial pressure (P/P_0) range of 0.05–0.3. The differential pore size distributions are also shown in Fig. 6 (b). These data showed that the samples exhibited H3 hysteresis type with non-uniform distribution of pores indicating that the nanoparticles are non-rigid aggregate of sheet or slit like particles as revealed by the SEM micrographs.

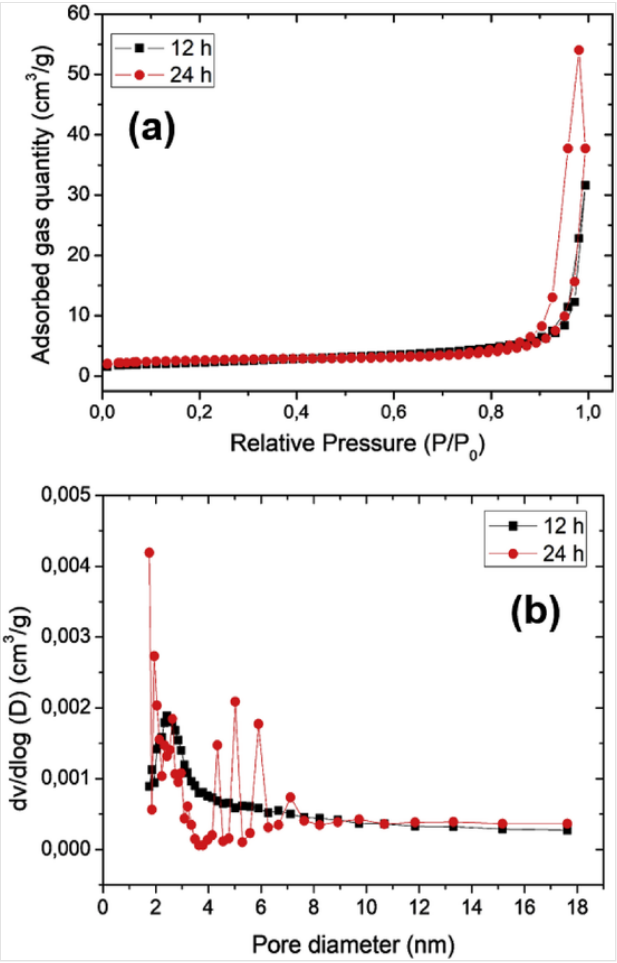

Fig. 6. (a) BET N_2 adsorption and desorption isotherms profiles of the nanopowders samples prepared at 12 and 24 h, (b) their respective BJH pore size distribution.

Gas sensing characteristics of the samples were analysed thoroughly as described in section 2.2 and the results are presented in Figs. 7 and 8. The dynamic response and recovery chemiresistive signals towards NH_3 gas of both samples presented in Fig. 7 demonstrated a promising sensing property for practical device development. Fig. 7 (a) is the signals acquired at the operating temperature of 350 °C while Fig. 7 (b) is the one taken at 400 °C. It is generally observed that the sample prepared for 12 h showed a slight superiority in response over the sample annealed for 24 h, especially at the higher temperature (400 °C). This is summarized in the sensor's responses and concentration profile and 60 ppm response versus operating temperature in Figs. 8 and 9 respectively. The sensor response in this work is defined as the relative change in the electrical property (current or resistance) of the V_2O_5 nanoparticles in the presence or absence of the analyte gas [27]. This slightly low sensing response displays in the case of the sample prepared at 24 h could be linked to its structural deformation and magnetic transition as well as the relatively bigger crystalline size. Theoretically, one would expect magnetic properties and sensing characteristics to share an inverse relationship since a material with well-aligned or oriented magnetic spins are likely to possess less surface defect, which normally play an important role in gas and chemical sensor's performance. It is also observed in Fig. 7 that the introduction of gas analyte resulted in an increasing current (decreasing resistance) through the sensors and it's withdraw decreases current (increases resistance) thereof. This is certainly true for the n-conductivity type;

V_2O_5 nanomaterial, and the reducing gas; NH_3 molecule [28]. Thus, the following processes are possible; when the V_2O_5 nanoparticles surface is exposed to the synthetic air present in the gas-sensing chamber, the materials surface would undergo a chemisorption process that will lead to the formation of adsorb oxygen (ionic species of oxygen) at the surface of the material. This process would rob the semiconductor of its conduction band electrons leading to decrease in current (increase in resistance) of the material. Now, when the material is exposed to NH_3, a reducing gas and an electron donor [19,20,27,28], the Fermi level of the material will shift towards the conduction band edge of the material leading to an increase in current and decrease in resistance. However, when the material is disengaged from NH_3 gas exposure, a reverse process would take place. The temperature dependent sensing response profile in Fig. 8 confirms Mott Hubbard's metal-to-insulator transition characteristics of V_2O_5 by exhibiting low response below 350 °C and high response above this transition temperature.

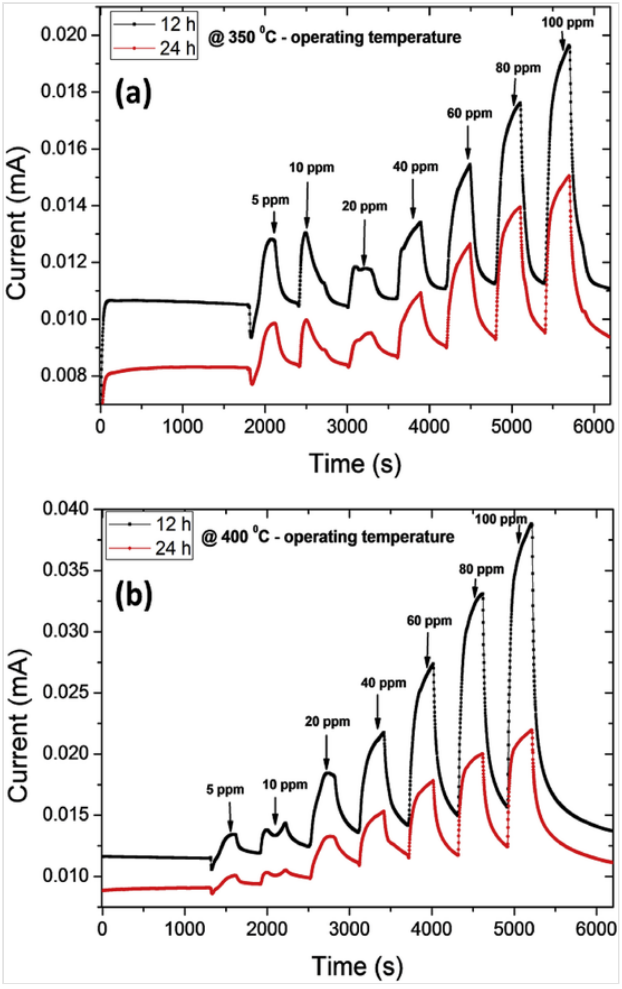

Fig. 7. Conductometric NH3 sensing signal of the samples prepared at 12 and 24, (a) operating temperature of 350 °C, (b) operating temperature of 400 °C.

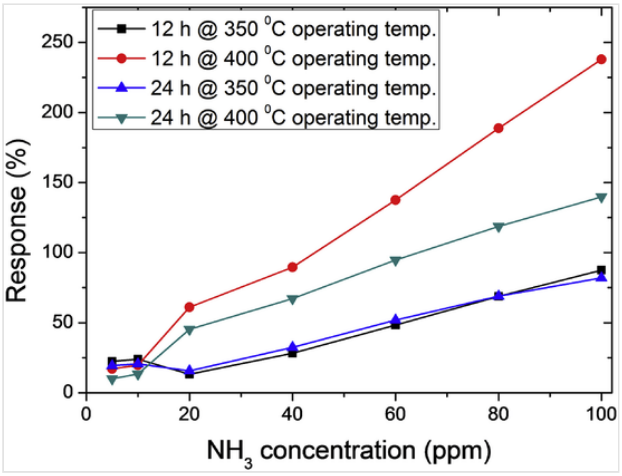

Fig. 8. Response profiles as a function of different gas concentrations.

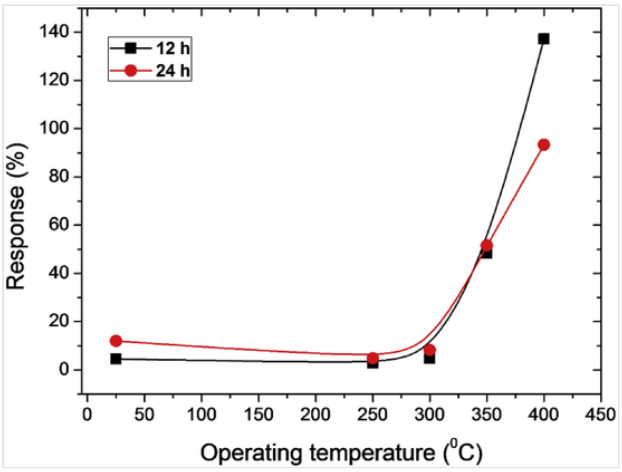

Fig. 9. Response versus operating temperature of 60 ppm concentration of NH_3.

Charge transfers and distributions, from DFT calculations, on V_2O_5 structure provided vital information on NH_3 gas sensing characteristics of the V_2O_5. Figs. 10–12 shows the adsorption of NH_3 molecule (s) and V_2O_5 interface and the charge density distribution in the surface-adsorbate system. As seen in Figs. 10 and 11, there was strong surface–adsorbate interaction, with Fig. 10 showing the accumulation of charges on the surface of α-V_2O_5 and depletion thereof from NH_3 molecules. The adsorption energy as a function of the number of NH_3 molecules was then obtained with the adsorption defined as;

$$E_a = E_{system} - E_{surface} - E_{adsorbate} \quad (1)$$

where E_{system} represents the total energy of the optimized V_2O_5 system, $E_{surface}$ is the total energy of the clean V_2O_5 surface and $E_{adsorbate}$ is the energy of the NH_3 gas. Negative values for E_a imply an exothermic reaction [29–31]. The calculated adsorption energies were all negative indicating that the surface-adsorbate systems were not only stable but also that the adsorption process was exothermic. From Fig. 12 (a), a decreasing linear pattern in the calculated adsorption energy per NH_3 is presented, showing that NH_3 exhibited less attraction (attractive force) with the increase in the numbers of NH_3 molecules. The normalized profile of adsorption energy per NH_3 in Fig. 12 (b) indicated that the (001), (200) and (400) surface have more active sites compared to the (110) surface. This profile also showed that the adsorption pattern is of Langmuir adsorption type which simulated the actual experimental sensing in Fig. 8.

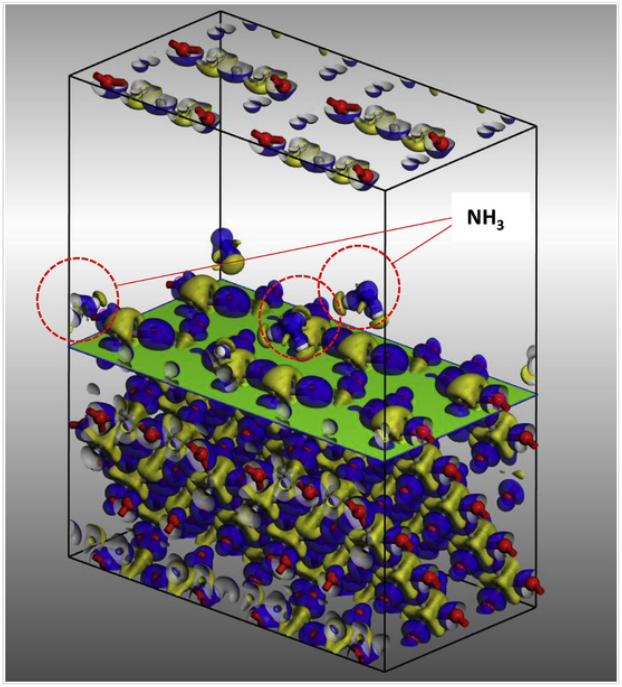

Fig. 10. Electron density difference of V_2O_5 (110) cleaved surface when exposed to NH_3 molecules. Blue shading shows charge accumulation while the yellow shading shows charge depletion.

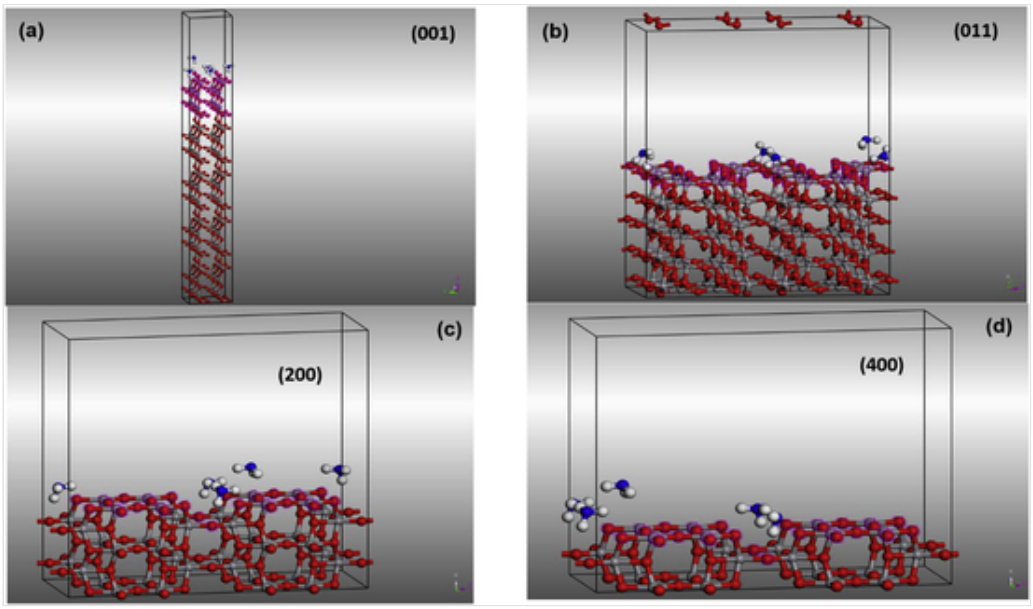

Fig. 11. Geometry optimized V_2O_5 planes (a) (001), (b) (110), (c) (200) and (d) (400) adsorbed with five NH_3 molecules.

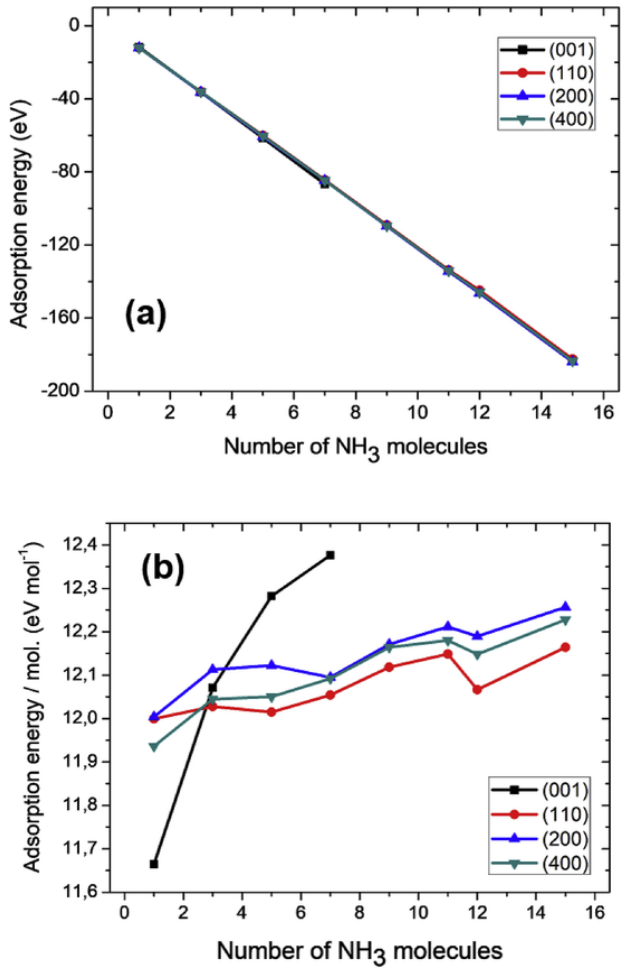

Fig. 12. (a) Calculated total adsorption energy versus number of NH_3 molecules, (b) plot of absolute values of adsorption energies per molecule versus number of NH_3 molecules. The number of adsorbed molecules is limited by the available adsorption sites in case of V_2O_5 (001) 2 × 2 supercell surface used.

The DFT calculated band structures are presented in Figs. 13 and 14 for systems with 3 NH_3 and 15 NH_3 molecules, respectively, while Fig. 15 shows the density of states (DOS) of V_2O_5 (110) surface adsorbed with NH_3 molecules, as well as the contribution of the NH_3 molecules to the total density of states. The band gap decreased exponentially with the increase in the number of adsorbed NH_3 molecules until it reached saturation around 12 NH_3 molecule loadings. When the number of NH_3 molecules is three (Fig. 13) a typical electronic band structure of the adsorbed NH_3 molecule(s) on V_2O_5 (110) obtained. From Fig. 14, a band gap reduction from ~2.2 eV of the clean bulk V_2O_5 system to about around 0.202 eV in the NH_3 adsorbed V_2O_5 (110) surface was observed when the number of NH_3 molecules is increased to 15. This decrease in the band gap can be explained by the occurrence of shallow DOS peak due to the presence of NH_3 molecules below the Fermi energy. The origin of NH_3 peak can be explained in terms of the hybridization of oxygen and hydrogen orbitals as evidenced by the charges density (Fig. 10). This observation of band gap decrease confirms the proposed sensing mechanism in which NH_3 molecules acts as electron donor by increasing the electron concentration and shifting the Fermi level towards the conduction band edge. This feature does not only corroborate the experimental response versus NH_3 concentrations (Fig. 8) but also the calculated adsorption energy per NH_3 molecules (Fig. 12).

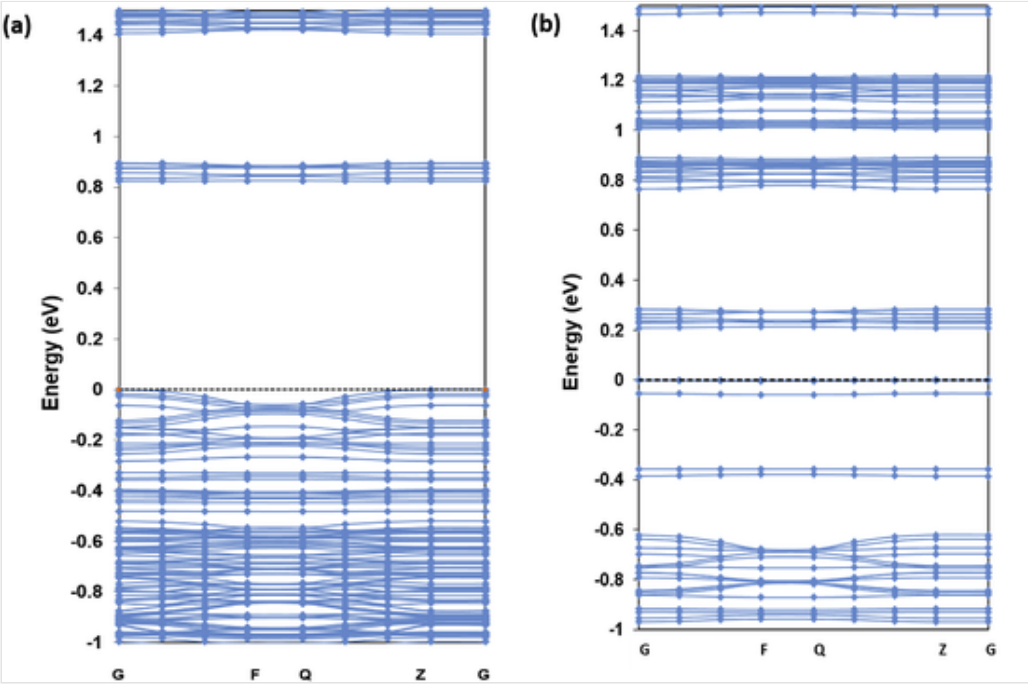

Fig. 13. Electronic band structure of V_2O_5 (110) cleaved surface adsorbed with (a) with 3 NH_3 molecules and (b) 15 NH_3 adsorbed molecules.

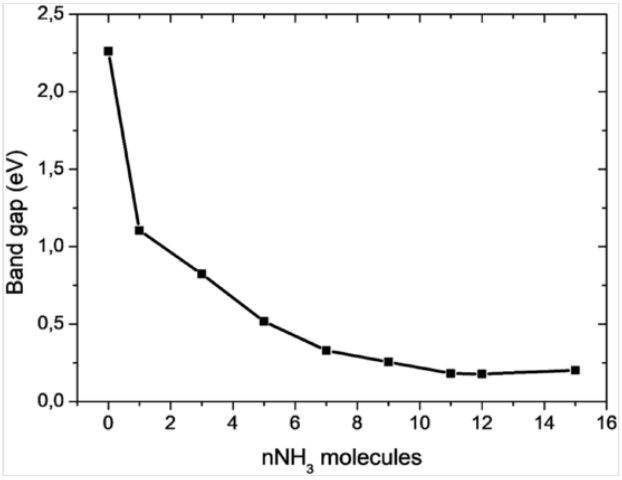

Fig. 14. Summary of the calculated electronic band gaps versus number of NH_3 molecules of NH_3 adsorbed V_2O_5 (110) surface.

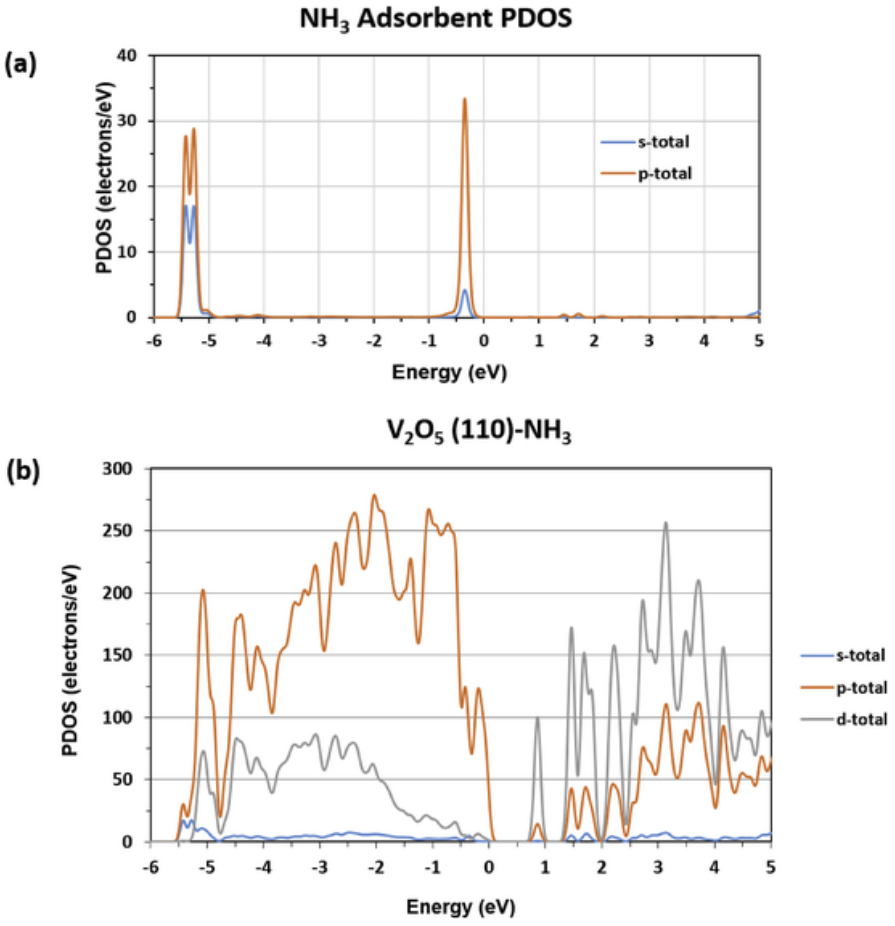

Fig. 15. Density of states V_2O_5 (110) surfaces adsorbed with 3 NH_3 molecules showing (a) the partial density of states of NH_3 (b) total density of states of the molecule adsorbed surface.

4 Conclusions

In summary, we have synthesized and characterized an orthorhombic α-V_2O_5 nano-rods structure and also modelled the system so as to study the NH_3 gas sensing and adsorption characteristics of the material. The crystallite sizes and micro/nano strain analyses of the material from XRD spectra showed that the sample prepared for 24 h in N_2 atmosphere is slightly deformed of larger crystals compared with the sample prepared for 12 h. This is also supported by the improvement in its magnetic properties as characterized by the VSM technique. The XRD spectral also showed that the (001) and (110) planes of the materials are dominant with high degree of crystallinity. The adsorption energies calculations of NH_3 gas molecule on orthorhombic α-V_2O_5 (110) cleaved surfaces indicated that the NH_3 molecules minimized their energies greatly on (001), (200) and (400) than (110) plane by exhibiting less energy. However, at higher concentration of NH_3 molecule, the (001) is likely to exhibit surface instability. The corresponding adsorption energies per NH_3 molecules against number of NH_3 molecules simulated the experimentally measured response pattern. Finally, the DFT calculated electronic band structure of the NH_3 adsorbed α-V_2O_5 (110) surface showed that the electronic band gap of the material's surface decreased exponentially with the increasing numbers of NH_3 molecules. These can be explained by the occurrence of defect state due to the NH_3 molecule in the V_2O_5 band gap as shown by the density of state profile. Overall, the NH_3 gas sensing characteristic of the sample composed of paramagnetic state having smaller crystal size, (sample prepared for 12 h) demonstrated high responses compared with the sample prepared for 24 h. These sensors showed significant rise in responses around the metal to insulator transition (MIT) temperature of the V_2O_5 material.

Author contribution

A. A. Akande; conceptualisation, methodology, experimental and theoretical data curation analyses, writing the original draft, submission and revision, C. N. M. Ouma and E.M. Benecha; theoretical data collection and analyses, T. Mosuang, T. Tesfamicheal, K. Roro, A. G. J. Machatine and B. W. Mwakikunga; data analyses, reviewing, editing and useful discussion.

Declaration of competing interest

Authors declare that there is no conflict of interest.

Acknowledgements

This work was funded by National Research Foundation through the Innovation Post-Doctoral Fellowship Grant of A. A. Akande, (Unique Grant No: 116749). Authors also thank CHPC for computational resources and CSIR for experimental facilities. Michael R. Horn at the Central Analytical Research Facility, Institute of Future Environments, Queensland University of Technology, Brisbane Australia is acknowledged for BET measurement.

References

[1] Tepper B., Richer B., Dupuis A.C., Kuhlenbeck H., Hucho C., Schilbe P., Yarmo M.A., Freund H.J., Adsorption of molecular and atomic hydrogen on vacuum cleaved V_2O_5 (001), Surf. Sci. 496 (2002) 64–72.

[2] Rao M.C., Vanadium pentoxide cathode material for fabrication of all solid state lithium-ion batteries - a case study, Res. J. Recent Sci. 2 (3) (2013) 67–73.

[3] Granqvist C.G., Electrochromic tungsten oxide films: review of progress 1993- 1998, solar energy mat, Sol. Cells 60 (2000) 201–262.

[4] Akande A.A., C Linganiso E., P Dhonge B., Rammutla K.E., Machatine A., Prinsloo L., Kunert H., Mwakikunga B.W., Phase Evolution of vanadium oxides obtained through temperature programmed calcinations of ammonium vanadate in hydrogen atmosphere and their humidity sensing, J. Mat. Chem. Phys. 151 (2015) 206.

[5] Akande A.A., Machatine A.G.J., Masina B., Chimowa G., Matsoso B., Roro K., Duvenhage M.-M., Swart H., Ray S.S., Mwakikunga B.W., Blue- and red- shifts of V_2O_5 phonons in NH_3 environment by in situ Raman Spectroscopy, J. Phys. D Appl. Phys. 51 (1) (2017) 105106.

[6] Huotari J., Spetz A.L., Lappalainen J., Gas sensing properties of pulsed laser deposited vanadium oxide thin films, The 14th International Meeting on Chemical Sensors, IMCS, 2012.

[7] Surnev S., Ramsey M.G., Netzer F.P., Vanadium oxide surface studies, Prog. Surf. Sci. 73 (4–8) (2003) 117–165.

[8] Zavahir S., Xiao Q., Zhao S.S.J., Bottle S., Wellard M., Jia J., Jing L., Huang Y., Blinco J.P., Wu H., Zhu H.Y., Selective oxidation of aliphatic alcohols using molecular oxygen at ambient temperature: mixed-valence vanadium oxide photocatalysts, ACS Catal. 6 (2016) 3580–3588.

[9] Imada M., Fujimori A., Tokura Y., Metal-insulator transitions, Rev. Mod. Phys. 70 (1998) 4.

[10] Schwingenschlögl U., Eyert V., The vanadium Magnéli phases V_nO_{2n-1}, Ann. Phys. 13 (9) (2004) 475.

[11] Kiria P., Hyettb G., Binions R., Solid-state thermochromic materials, Adv. Mater. Lett. 1 (2) (2010) 86–105.

[12] Eyert V., The metal-insulator transitions of VO_2: a band theoretical approach, Ann. Phys. 11 (9) (2002) 1–61.

[13] Rao M.C., Structural stoichiometry and phase transitions of MoO_3 thin films for solid state microbatteries, Res. J. Recent Sci. 2 (2013) 3.

[14] Laubach S., Schmidt P.C., Thiben A., Fenandez-Madrigal F.J., Wu Q., Jaegemann W., Klemm M., Horn S., Theoretical and Experimental determination of the electronic structure of V_2O_5, reduced V_2O_{5-x} and sodium intacalated NaV_2O_5, Phys. Chem. Chem. Phys. 9 (2007) 2564.

[15] Schmitt T., Augustsson A., Nordgren J., Dudaa L.-C., Höwing J., Gustafsson T., Schwingenschlögl U., Eyert V., Electronic structure of Li-inserted V_6 O_{13} battery cathodes: rigid band behavior and effects of hybridization, Appl. Phys. Lett. 86 (2005) 064101.

[16] Hejduk P., Witko M., Hermann K., Electronic structure of unsaturated V2O5(001) and (100) surfaces: ab initio density functional theory studies, Top. Catal. 52 (2009) 1105–1115.

[17] Chakrabarti A., Hermann K., Druzinic R., Witko M., Wagner F., Petersen M., Geometric and electronic structure of vanadium pentoxide: a density functional bulk and surface study, Phys. Rev. B. 59 (16) (1999) 10 589.

[18] Yin X., Fahmi A., Han H., Endou A., Salai Cheettu Ammal S., Kubo M., Teraishi K., Miyamoto A., Adsorption of H_2O on the V2O5(010) surface studied by periodic density functional calculations, J. Phys. Chem. B 103 (1999) 3218–3224.

[19] Akande A.A., Mwakikunga B.W., Rammutla K.E., Machatine A., Larger selectivity of the V_2O_5 nano-particles sensitivity to NO_2 than NH_3, Sens. Tran. 192 (2015) 9.

[20] Akande A.A., Rammutla K.E., Dhonge B.P., Machatine A.G.J., Mwakikunga B.W., Room temperature Methane (CH_4) sensing by vanadium oxide (VO_x) nanoparticles, Adv. Sci. Lett. 22 (2016) 901–904.

[21] Qin Y., Fan G., Liu K., Hu M., Vanadium pentoxide hierarchical structure networks for high performance ethanol gas sensor with dual working temperature characteristic, Sens. Actuators B 190 (2014) 141–148.

[22] Yin X., Han H., Gunji I., Endou A., Ammal S.S.-C., Kubo M., Miyamoto A., NH_3 adsorption on the bronsted and lewis acid sites of V_2O_5 (010): a periodic density functional study, J. Phys. Chem. B 103 (1999) 4701–4706.

[23] Clark S.J., Segall M.D., Pickard C.J., Hasnip P.J., Probert M.J., Refson K., Payne M.C., Kristallogr Z., First principles methods using CASTEP, 220 (2005) 567.

[24] Perdew J.P., Burke K., Ernzerhof M., Generalized gradient approximation made simple, Phys. Rev. Lett. 77 (1996) 3865.

[25] Vanderbilt D., Soft self-consistent pseudopotentials in a generalized eigenvalue formalism, Phys. Rev. B 41 (1990) 7892.

[26] Ruiyu J., Dengyang L., Chao C., Zhu T., Fanfan Y., Jinhong Z., Adsorption simulation of sulfur oxide on the surface of metal, J. Chem. Pharm. Res. 6 (3) (2014) 949–954.

[27] Mwakikunga B.W., Motshekga S., Sikhwivhilua L., Moodley M., Scriba M., Malgas G., Simo A., Sone B., Maazad M., e, Ray S.S., A classification and ranking system on the H_2 gas sensing capabilities of nanomaterials based on proposed coefficients of sensor performance and sensor efficiency equations, Sens. Actuators B 184 (2013) 170–178.

[28] Watchakun K., Samerjai T., Tamaekong N., Liewhiran C., Siriwong C., Kruefu V., Wisitsoraat A., Tuantranont A., Phanichphant S., Semiconducting metal oxides as sensor for environmentally hazardous gases, Sens. Actuators B. 160 (2011) 580–591.

[29] Ng M.-F., Teo M.K., Lim K.H., Zhou L., Sullivan M.B., Yang S.-W., Towards tuning of surface properties by atomic and molecular adsorption on boron-terminated cubic boron nitride (111) surface: a first-principles study, Diam. Relat. Mater. 17 (2008) 2048–2053.

[30] Kulish V.V., Ng M.-F., Malyi O.I., Wu P., Chen Z., Enhanced Li adsorption and diffusion in single-walled silicon nanotube: an ab inito study, ChemPhysChem 14 (6) (2013) 1161–1167.

[31] Leenserts O., Partoens B., Peeters F.M., Adsorption of H_2O, NH_3, CO, NO_2 nad NO: a first-principle study, Phys. Rev. B 77 (2008) 125416.

Highlights

- Para-to ferro-magnetic transition behaviour of the Orthorhombic α-V_2O_5 nano-rods particles.
- Excellent NH_3 gas response property in the vicinity of α-V_2O_5's metal-to- insulator transition temperature.
- Observation of inverse relationship of magnetic and NH_3 sensing property of α-V_2O_5 nano-rods particles.
- Correlation of DFT adsorption energy's profile and the actual experimental sensing response of α-V_2O_5.
- Reduction in the surface electronic band gap with increasing number of adsorbed NH_3 molecules.